Water Air Soil Pollut (2018) 229: 109
https://doi.org/10.1007/s11270-018-3768-3

Preparation and Denitration Performance of V-W/TiO_2-SiO_2 Nanotube Catalysts

Kezhi Zheng · Guohua Yang · Weijie Shen · Qingtao Xu · Fuxiang Hu · Zhen Li

Received: 8 November 2017 / Accepted: 28 February 2018 / Published online: 8 March 2018

Abstract TiO_2-SiO_2 nanotubes, with high specific surface area, were prepared by hydrothermal methods using tetraethyl orthosilicate and tetrabutyl titanate as precursors. These nanotubes were used as carriers to prepare a V_2O_5-WO_3/TiO_2-SiO_2 catalyst by an impregnation method. The deNO$_x$ activity of catalysts used for selective catalytic reduction (SCR) was examined as a function of the silica-to-titania molar ratio, vanadium loading, and calcination temperature. The catalyst performance was also tested in the presence of sulfur and water. The experimental results showed that the nanotube catalyst loaded with 3 wt% vanadium and a SiO_2/TiO_2 molar ratio of 2:8 exhibited the best activity after calcination at 650 °C. The NO conversion efficiency reached 100% at a gas hourly space velocity (GHSV) of 100,000 h^{-1} over the reaction temperature range of 300–500 °C. Characterization by Brunauer–Emmett–Teller measurements, X-ray diffraction, transmission electron microscopy, temperature-programmed reduction, and temperature-programmed desorption demonstrated that formation of the nanotube structure significantly increased the specific surface area of the catalyst and that the active components exhibited high degree of dispersion on the carrier. Moreover, SiO_2 doping enhanced the number of acidic sites on the catalyst surface while inhibiting anatase-to-rutile phase transformation, resulting in a wider temperature window for catalytic activity and higher NO$_x$ conversion efficiency.

K. Zheng · G. Yang (✉) · W. Shen · Q. Xu · F. Hu · Z. Li
Faculty of Maritime and Transportation, Ningbo University, Ningbo, Zhejiang 315211, China
e-mail: yangguohua@nbu.edu.cn

Keywords Selective catalytic reduction · deNO$_x$ catalyst · Silicon-doped titanium nanotube · Antipoisoning performance

1 Introduction

Nitrogen oxide (NO$_x$) is one of the major exhaust pollutants derived from diesel engines. NO$_x$ discharges into the atmosphere can cause a series of environmental problems such as acid rain and photochemical smog, posing a significant risk to human health (Weber et al. 2010; Morin et al. 2008). Selective catalytic reduction (SCR) is thus far the most mature and effective technology for denitration (deNO$_x$), having the advantages of high NO$_x$ conversion efficiency, good selectivity, and low requirement for fuel sulfur content (Forzatti 2001; Pang et al. 2014). The key to SCR technology is the selection of catalysts with good performance. Currently, V_2O_5-WO_3 (MoO_3)/TiO_2 is widely used as a commercial catalyst. Vanadium-based catalysts possess various advantages, including high activity, good selectivity, and excellent water- and sulfur-resistant performance (Cheng et al. 2014); however, since V_2O_5 is toxic and can oxidize SO_2 to form SO_3 (Madia et al. 2002; Kristensen et al. 2011), commercial catalysts generally contain less than 2% vanadium (Vedrine 2000). Vanadium-based catalysts have the disadvantages of narrow reactive windows and deactivation at high temperatures (Odenbrand 2008; Madia et al. 2002; Zhang et al. 2014). These catalysts exhibit good activity only at 300–400 °C, and are deactivated due to their poor

thermal stabilities. Exposure of these catalysts to high-temperature gases not only results in TiO_2 sintering, which transforms anatase TiO_2 into the inactive rutile phase, but also volatilizes vanadium–tungsten active substances (Nova et al. 2001; Choung et al. 2006).

Many researchers have attempted to address the shortcomings of vanadium-based catalysts. For example, composite oxides such as TiO_2-SiO_2, TiO_2-Al_2O_3, and TiO_2-ZrO_2 were used as supports to improve the thermal stability of vanadium-based catalysts with significant enhancement of TiO_2 support performance using SiO_2 (Jin et al. 2009; Shi et al. 2011). Kobayashi et al. (2005) prepared monolithic catalysts using TiO_2-SiO_2 as the support and compared their performance with that of pure TiO_2-supported catalysts. They revealed that the SiO_2 addition increased the Brunauer–Emmett–Teller (BET) surface area, the number of acidic sites, and the thermal stability of the catalyst. Liu et al. (2016) reported that SiO_2 addition inhibited the phase transition of TiO_2 from anatase to rutile, the increase in TiO_2 crystallite size, and the reduction in the specific surface area of the catalyst, thereby improving the stability of the V_2O_5/WO_3-TiO_2 catalyst. Wang and Sun (2011) found that the introduction of a small amount of Si into TiO_2 not only hindered the increase in TiO_2 particle size and phase transformation but also generated Ti^{3+} ions near the catalyst surface during the thermal diffusion of Si and Ti atoms, thus promoting the photocatalytic degradation of methyl orange. TiO_2 nanotubes have a larger surface area than nanoparticles, which could enhance dispersion of the active components (Yao et al. 2011) and thus the catalytic efficiency. Chen et al. (2012) found that the NO conversion efficiency of ceria-loaded titanate nanotube catalysts synthesized using the hydrothermal method was 100% at a reaction temperature of 350 °C, which was 22% higher than that of the catalysts supported by titanate nanoparticles. Wang et al. (2011) prepared titanium nanotube (TNT)-confined ceria and found that the active component, CeO_2, not only existed on the outer surface of the support but also accumulated inside the TiO_2 nanotubes. Compared with catalysts supported by TiO_2 nanoparticles, the CeO_2-loaded TiO_2 nanotube catalysts showed higher NO conversion efficiency and a wider reaction temperature window. Fang et al. (2007) synthesized SiO_2-TiO_2 nanotubes for calcination at 500 °C. An X-ray diffraction (XRD) analysis demonstrated that the SiO_2-TiO_2 nanotubes were in the anatase phase, with smaller diameter and larger specific surface area than anatase TiO_2 nanotubes. Under the same light intensity of 450 μW/cm^2, the processing speed of acid orange II in SiO_2-TiO_2 nanotubes was 12% higher than that in TiO_2 nanotubes after 120 min of reaction.

Previous studies demonstrated that both Si doping and nanostructure formation may improve the catalytic activity. In our tests, a series of V_2O_5-WO_3/TiO_2-SiO_2 nanotube catalysts were prepared to examine the NO conversion activity of SCR catalysts as a function of the silica-to-titania molar ratio, vanadium loading, and calcination temperature and to evaluate catalyst performance in the presence of sulfur and water.

2 Experiments

2.1 Catalyst Preparation

2.1.1 Preparation of Titanium Silicon Composite Nanoparticles through Coprecipitation

At 40–50 °C, tetraethyl orthosilicate was added to a 17.4 wt% nitric acid solution, and stirred vigorously until it was completely hydrolyzed and a transparent solution was obtained. During stirring, tetrabutyl titanate was added dropwise to the above solution. The molar ratio of tetraethyl orthosilicate and tetrabutyl titanate/HNO_3/H_2O was 1:2:50, where six samples with SiO_2/TiO_2 molar ratios of 0:10, 1:9, 2:8, 3:7, 4:6, and 5:5 are herein referred to as 1–6#NP (NP is short for nanoparticle), respectively, according to the molar ratios. After continuous stirring for 15 min, the solution was left to stand for ~ 10 min to allow the solution to separate into layers. The organic upper layer was removed, and the solution was left to stand at 50 until the white powder precipitated. Then, the white powder was filtered and dried at 110 °C. Finally, the sample was calcined for 5 h at 500 °C and ground into white powder to obtain nanoparticles with different SiO_2/TiO_2 molar ratios.

2.1.2 Hydrothermal Synthesis of SiO_2-TiO_2 Nanotubes

First, a 10 mol/L NaOH solution was prepared and vigorously stirred for 2 h, during which a certain amount of TiO_2-SiO_2 nanoparticles was added. Second, the temperature of the solution was increased to 130 °C in a drying oven at the rate of 1 °C/min and taken out after 24 h of thermal insulation. Third, the sample was

naturally cooled to ambient temperature and separated via centrifugation. Next, the lower layer sediment was washed by deionized water to obtain neutral pH before acid washing using a 0.1 mol/L HCl solution. Then, Cl^- and Na^+ were removed using deionized water. The sample was then dried in the oven at 80 °C. The temperature of the sample was increased to 350 °C at a rate of 1 °C/min, after which the sample was calcined for 2 h. After cooling, six TiO_2-SiO_2 nanotube samples, hereafter referred to as 1–6#NT (NT is short for nanotube), were obtained through grinding.

2.1.3 Preparation of Catalysts Using an Impregnation Method

Ammonium metavanadate and ammonium tungstate were dissolved in 50 mL deionized water, and a certain amount of TiO_2-SiO_2 nanotubes were added to the solution. After the solution was intensively stirred for 2 h, the sample was dried in a drying oven at 80 °C. After 3 h of calcination at a certain temperature, the sample was cooled for tableting and catalyst particles of 40–60 mesh size were selected. The amounts of ammonium metavanadate and ammonium tungstate were calculated according to the mass fractions of V_2O_5 and WO_3 in the raw materials. V_2O_5 loading amounts in the samples were 0.5, 1, 2, and 3 wt%, while the WO_3 loading was 10 wt%. The samples are referred to in the text as mV-10W/n#NT-T, where the V_2O_5 loading is represented by $m = 0.5–3$, the support sample number is $n = 1–6$, and the catalyst calcination temperature is $T = 350–650$ °C.

2.2 Catalyst Characterization

Catalyst-phase structures were analyzed using an X-ray diffractometer (XRD; D8 Advance, Bruker AXS, Germany), with the voltage of the X-ray tube with a Cu target ≤ 50 kV, current of the tube ≤ 40 mA, goniometer precision = 0.0001°, goniometer accuracy ≤ 0.02°, and scanning range 2θ = 10–80°. The BET surface area of the catalyst was measured using the N_2 adsorption method on a fully automated physisorption/chemisorption analyzer (ASAP 2020 M, Micromeritics, USA). Catalyst morphology and microstructures were observed using a transmission electron microscope (TEM) (JEOL 2100HR, JEOL, Japan).

Hydrogen temperature-programmed reduction (H_2-TPR) tests were conducted using a fully automated chemisorption analyzer (AutoChem II 2920, Micromeritics, USA). In the tests, 100 mg of sample was preprocessed in He gas at 400 °C for 1 h and then cooled to 50 °C in a He atmosphere. Subsequently, the gas inlet was switched from He to H_2. The sample was left to stand for 30 min, and the temperature was increased to 800 °C at a heating rate of 10 °C/min. Then, the H_2 content in the exhaust was measured using a thermal conductivity detector (TCD).

Ammonia temperature-programmed desorption (NH_3-TPD) tests were implemented using AutoChem II 2920 (Micromeritics, USA). Sample (100 g) was preprocessed in He at 400 °C for 1 h and then cooled to 50 °C in a He atmosphere. NH_3 was introduced in the chamber for the sample to adsorb. After 30 min of adsorption, the sample temperature was then increased to 800 °C at a heating rate of 10 °C/min, and the NH_3 desorption curve was recorded.

2.3 Catalyst Evaluation

The activity tests for SCR catalysts were conducted on the in-house catalytic reaction device. A quartz glass tube with an internal diameter of 6 mm was adopted as the reactor, which was heated by a tube furnace. Simulated diesel engine exhaust was composed of 1000 ppm NO, 1000 ppm SO_2, 1000 ppm NH_3, 5% O_2, and 5% H_2O, with N_2 as the carrier gas. The gases were controlled by mass flow meters. NO concentration was detected online using a Gasboard 3000 flue gas analyzer (China). In order to avoid the effect of adsorption on the activity characterization data, each test point was recorded after allowing the sample to stand for 0.5 h. The catalyst activity was presented using the NO conversion efficiency.

3 Results and Discussion

3.1 Activity Measurements

3.1.1 Impact of SiO_2/TiO_2 Ratio in the Support

Figure 1 shows the NO conversion efficiencies of the SCR reaction for the 1–6# nanotube catalysts. The NO conversion efficiencies first increased with increasing SiO_2 content in the support, then decreased, and finally peaked when the SiO_2/TiO_2 molar ratio in the support was 1:9. The catalyst supports with respect to NO conversion efficiency are ranked from highest to lowest as

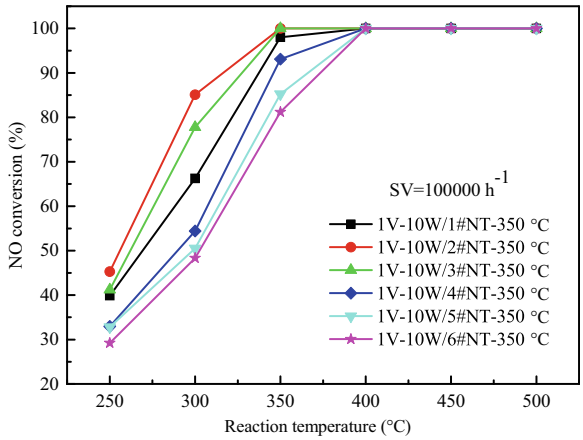

Fig. 1 Impact of support on catalytic activity

follows: 2#NT, 3#NT, 1#NT, 4#NT, 5#NT, and 6#NT, demonstrating that an appropriate amount of Si can improve catalytic activity, whereas excessive Si doping can reduce the catalyst's NO conversion efficiency. As indicated by the BET and XRD data, Si doping can increase the catalyst's specific surface area, block the generation of rutile-phase TiO_2 (Shen and Ma 2012), promote the dispersion of V_2O_5, and therefore enhance the catalyst activity. However, excess SiO_2 caused NH_3 to adsorb on a large number of acidic sites, impeding the effective transformation of NO into N_2, thereby retarding the SCR reaction (Jin et al. 2009). Moreover, VO_x is difficult to reduce due to the strong interactions between vanadium oxide and silicon dioxide on the catalyst surface, which decreases the catalyst activity (Gao et al. 1999).

3.1.2 Impact of Vanadium Loading

Figure 2 illustrates the decrease in NO conversion efficiency of the nanotube catalysts with increasing vanadium loading. Figure 2a shows that the NO conversion efficiency of TiO_2 nanotube catalysts increased as the reaction temperature was increased from 250 to 450 °C. When the reaction temperature was higher than 450 °C, all the catalysts showed reduction in NO conversion efficiency to different degrees, except for the catalyst with 1 wt% vanadium loading. This is due to the oxidation of NH_3 at high temperatures, i.e., $4NH_3 + 5O_2 \rightarrow 4NO + 6H_2O$, $2NH_3 + 2O_2 \rightarrow N_2O + 3H_2O$, and $4NH_3 + 3O_2 \rightarrow 2\,N_2 + 6H_2O$, which not only consumes the NH_3 participating in the SCR reaction but also generates NO (Camposeco et al. 2014). Moreover, the SCR moves toward the low-temperature zone with

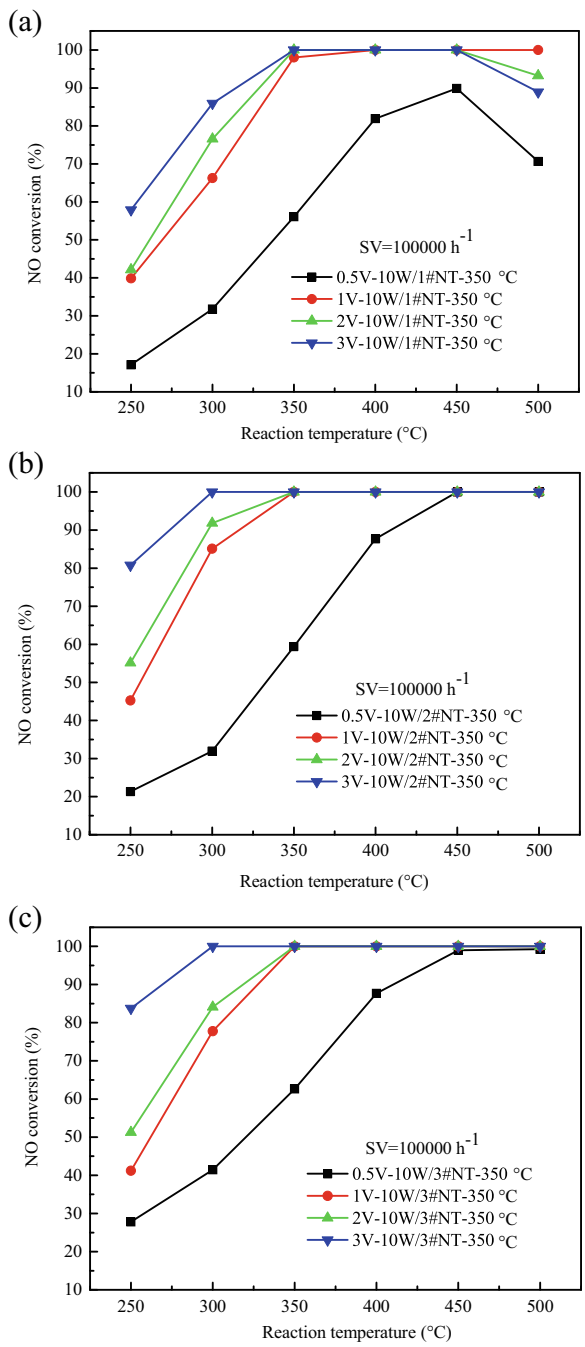

Fig. 2 Impact of vanadium loading on catalyst activity

increasing V_2O_5 content, indicating that a high concentration of vanadium oxide as the primary activity center of SCR reaction promotes NH_3 activation (Zhao et al. 2010). By comparing Fig. 2b, c to Fig. 2a, we can see that the NO conversion efficiency of SiO_2-doped nanotube catalysts was significantly improved. The NO

conversion efficiency of the 3 wt% vanadium-loaded catalyst reached 100% at a reaction temperature of 300 °C, and the denitration efficiency of the catalyst did not decrease even at reaction temperatures higher than 450 °C. This is probably because the addition of SiO_2 could inhibit the oxidation of NH_3, and therefore enhance the high-temperature activity of the catalyst.

3.1.3 Impact of Calcination Temperature

Figure 3 shows the variation in NO conversion efficiency of the SCR reaction for various nanotube catalysts with respect to calcination temperature. In Fig. 3a, TiO_2 nanotubes act as the catalyst support. The catalyst calcined at 450 °C shows 100% NO conversion efficiency in the reaction temperature range 300–500 °C. On the other hand, the worst NO conversion efficiencies (< 70% over the entire reaction temperature range) are observed for the catalysts calcined at 650 °C. This is because the titanate nanotube structure was destroyed during the high-temperature calcination at 650 °C, which reduced the specific surface area and V_2O_5 dispersity of the catalyst, resulting in a substantial decrease in the NO conversion activity (Tang et al. 2013). When 10 mol% SiO_2 was present in the nanotube catalyst (Fig. 3b), the variation in nanotube catalyst activity displays a trend similar to that shown in Fig. 3a. However, the nanotube catalysts in Fig. 3c, which contain 20 mol% SiO_2, experienced a significant improvement in their NO conversion activity, which was higher than 80% over the broad reaction temperature region of 250–500 °C. Specifically, the NO conversion efficiency of the catalyst calcined at 650 °C stayed at 100% over the entire reaction temperature range. Compared to Fig. 3a, the NO conversion efficiency in Fig. 3b, c was enhanced and NO conversion efficiency of the catalyst was not reduced even at reaction temperatures higher than 450 °C, which further demonstrates that an appropriate amount of doped Si can improve the thermal stability of catalyst. This is because doping with SiO_2 inhibits the conversion of anatase TiO_2 to the inactive rutile TiO_2 phase and the destruction of the catalyst (Wang and Sun 2011; Chen et al. 2012), which is also verified by the characterization results described below.

3.1.4 Impact of H_2O and SO_2

H_2O- and SO_2-resistant performance was evaluated using the 3V-10W/3#NT-650 °C catalyst. The reaction

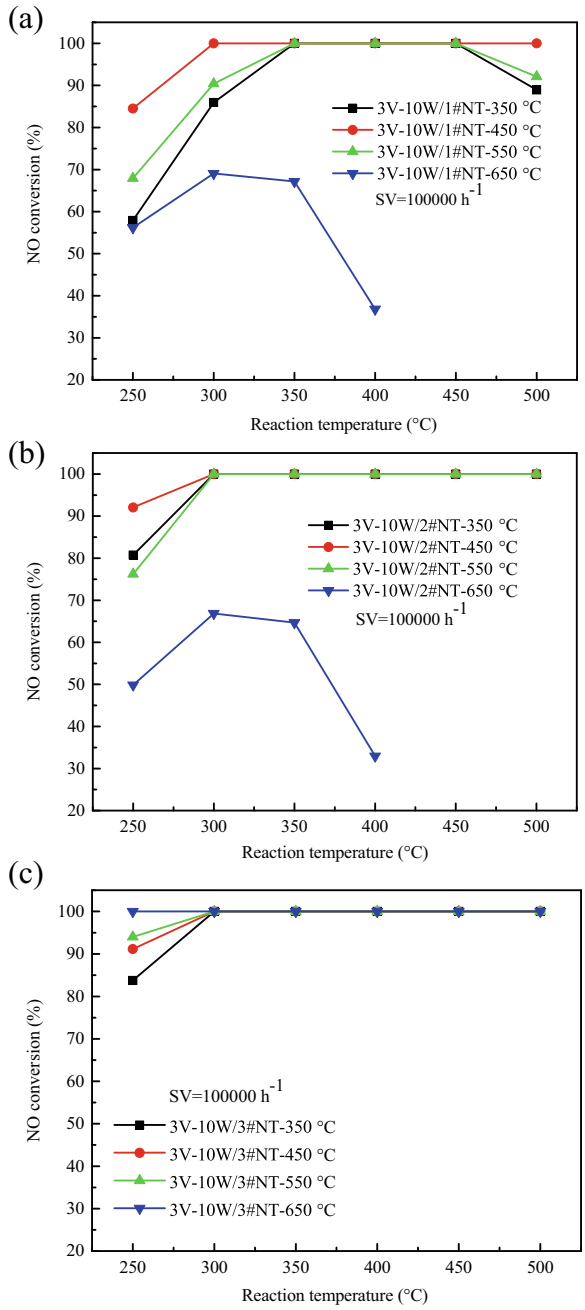

Fig. 3 Impact of calcination temperature on NO conversion activity

proceeded under the conditions of simulated exhaust without water and sulfur for 1 h. Then water resistance tests were conducted.

As shown in Fig. 4, the NO conversion efficiency remains 100% in the absence of water but reduces to 93% after the introduction of 5% H_2O. This is because during the SCR reaction, competitive adsorption takes

place between H_2O and NH_3 on the catalyst surface, hindering the reaction of NH_3 and NO (Huang et al. 2006). The reaction approached equilibrium 60 min after water injection, and the NO conversion efficiency reverted to 100% after the water injection was stopped. In other words, the inhibitory effect of H_2O on the catalyst was reversible. Under the same reaction conditions, sulfur resistance tests were conducted by introducing SO_2. Figure 4 shows that the NO conversion efficiency was not influenced by the introduction of SO_2, as it remained 100%, because SiO_2 inhibits the oxidizability of SO_2 (Tran et al. 2016), and the nanotube structure protected the active components. When 5% H_2O and 1000 ppm SO_2 were simultaneously introduced at a reaction temperature of 280 °C, the NO conversion efficiency of the catalyst gradually dropped to 90.36%, lower than that when only H_2O was introduced into the catalyst. This is mainly because H_2O accelerated ammonium sulfate formation. The formation speed was higher than the decomposition speed at a reaction temperature of 280 °C; thus, the ammonium sulfate gradually covered the catalyst surface, reducing the NO conversion efficiency. However, the efficiency was still significantly higher than that of the V_2O_5-WO_3/TiO_2 catalyst at the same temperature (Tao et al. 2008). The NO conversion increased to 97% after the introduction of H_2O, and SO_2 was stopped because some ammonium sulfate was deposited on the catalyst surface and was difficult to decompose at 280 °C (Fan and Cao 2011). When 5% H_2O and 1000 ppm SO_2 were simultaneously introduced at a reaction temperature of 300 °C, the NO conversion efficiency of the catalyst was significantly improved and reverted to 100% after water injection was stopped. This indicted that the increase in temperature can weaken the effect of water and SO_2 on the catalyst.

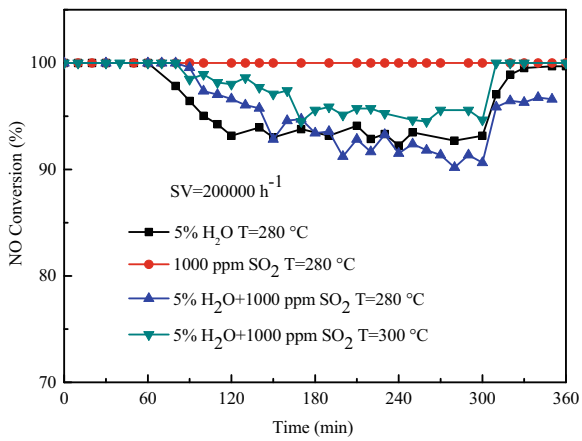

Fig. 4 Impact of H_2O and SO_2 on NO conversion activity

3.2 Catalyst Characterization Results

3.2.1 BET Analysis

As indicated in Table 1, the BET surface area of SiO_2-doped nanotube catalysts can reach 130.12 and 109.65 m^2/g after calcination at 450 and 650 °C, respectively. The surface area declined with increasing calcination temperature. XRD analysis revealed that a portion of the nanotubes in the catalyst were destroyed when the calcination temperature was 650 °C, causing the reduction in the catalyst's BET surface area. The BET surface area of the 3V-10W/3#NT-650 °C catalyst was more than 2.5 times that of 3V-10W/3#NP-650 °C, demonstrating that the nanotube structure can dramatically increase the catalyst's BET surface area. However, the BET specific surface area of the nanotube catalyst without Si addition after calcination at 650 °C was only 16.08 m^2/g, much smaller than that of the 3V-10W/3#NT-650 °C catalyst prepared under the same conditions.

3.2.2 XRD Analysis

Figure 5 shows the XRD spectra of the catalysts. All the four types of catalysts demonstrate the peaks of anatase TiO_2 (PDF 21-1272). The three catalyst samples without added Si did not show XRD peaks corresponding to rutile TiO_2 and WO_3, while the 3V-10W/1#NT-650 °C catalyst showed XRD peaks corresponding to rutile TiO_2 and WO_3, indicating that Si addition can improve the thermal stability of the catalysts, can inhibit the transition of TiO_2 from anatase phase to rutile phase, and can enhance the dispersion of WO_3 on the support surface. In addition, the three catalyst samples with added Si did not show the characteristic peaks of SiO_2, demonstrating that SiO_2 was amorphous (Dong et al.

Table 1 BET surface area of the catalysts

Sample	S_{BET} (m^2/g)
3V-10W/3#NT-450 °C	130.12
3V-10W/3#NT-650 °C	109.65
3V-10W/3#NP-650 °C	43.76
3V-10W/1#NT-650 °C	16.08

2016). Compared to 3V-10W/3#NT-450 °C, 3V-10W/3#NT-650 °C exhibited a narrower and sharper diffraction peak for anatase TiO_2, indicating that the anatase phase of the catalyst prepared by calcination at 650 °C had higher crystallinity and larger crystallite size, which is in agreement with the catalyst's BET results. The crystallinity of 3V-10W/3#NT-650 °C was higher than that of 3V-10W/3#NP-650 °C possibly because some Si was lost in the hydrothermal treatment and washing steps of the TiO_2-SiO_2 nanotube synthesis. Su et al. (2008) indicated in their study that Si might be incorporated into the titania matrix, which helped increase the thermal stability of titania, thereby suppressing the phase transformation from anatase into rutile and inhibiting the growth of anatase crystallites at high calcination temperatures.

3.2.3 SEM Analysis of Supports

Figure 6 shows the SEM images of different supports after calcination at 350 °C. It can be seen from Fig. 6a, b that Ti prepared by the coprecipitation method and the support with a Ti/Si molar ratio of 8:2 were in the form of nanoparticles. The particle diameter of Ti nanoparticles was 15–25 nm, and some caking was also observed, with uneven particle size; after Si addition to 3#NP, its particle size became more uniform and its particle diameter became smaller than those of 1#NP. Since Si atoms will enter the Ti lattice, exerting a curing effect on the crystal structure of Ti and reducing the atomic spacing, the particle diameter will be relatively reduced. The scan images of 1#NT and 3#NT (Fig. 6c, d, respectively) show that after the hydrothermal reaction, the supports showed a thin strip structure, with diameter of 10–15 nm. According to the cross sections and intersection points of the strip structure, it was a hollow structure, indicating that a nanotube structure was prepared by the hydrothermal reaction. By comparing Fig. 6c, d, we can find that the tube diameter of 3#NT was slightly smaller than that of 1#NT, and the structure of the tube was clearer. Due to the decrease in particle size after Si addition, the tube diameter of the nanotube structure formed by hydrothermal synthesis was relatively small.

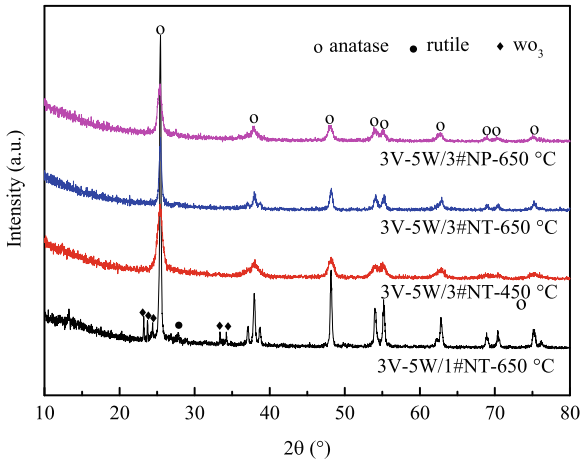

Fig. 5 XRD spectra of the prepared catalysts

3.2.4 TEM Analysis

Figure 7 shows the TEM images of the catalysts. Figure 7a, b shows the typical morphology of the 3V-10W/3#NT catalyst after calcination at 450 °C. It can be observed that although the nanotubes are bonded to each other, the nanotube structure remained intact, without any particle inside the nanotubes. This demonstrates that the V-W active elements were uniformly distributed on the surface of the support without agglomeration or sintering. Figure 7c, d shows TEM images of the 3V-10W/3#NT catalyst after calcination at 650 °C. These figures show that agglomeration occurred in the catalyst, making the tube structure less obvious. However, the BET surface area of the catalyst was larger than that based on catalysts supported by SiO_2-TiO_2 nanoparticles (43.76 m^2/g), indicating that although 3V-10W/3#NT-650 °C experienced a certain degree of burning damage, it was not completely burnt to form particles or nanorods. It can also be seen that the catalyst contained relatively wide strips and slices in its morphology, along with some nanotubes.

3.2.5 H_2-TPR Analysis

H_2-TPR is generally used to characterize the redox ability of the catalysts and the interaction between the surface-active substances and their supports. It can be observed from Fig. 8 that the catalyst has three broad peaks (3V-10W/3#NT-650 °C catalyst has a reduction peak at 801.4°) that indicate the reduction of V_2O_5 and WO_3 (Liu et al. 2016). V_2O_5 and WO_3 possess different reduction properties on the TiO_2-SiO_2 support, illustrating that they have different interactions with the support (Wang et al. 2013). The reduction peaks at 450–550 °C are due to the joint action of the reduction of V^{5+} to V^{3+} and of W^{6+} to W^{4+} (Putluru et al. 2016), whereas the reduction peak at 670–730 °C is due to the reduction of

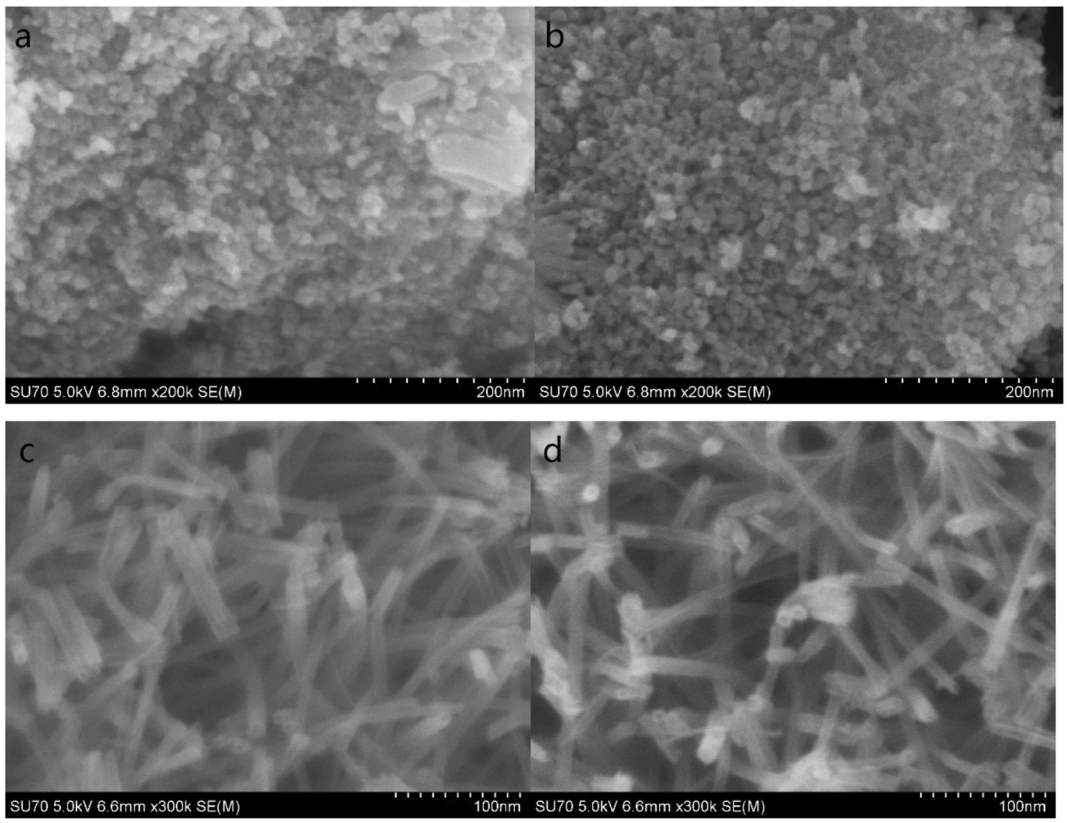

Fig. 6 Surface morphology of different supports. **a** 1#NP-350 °C. **b** 3#NP-350 °C. **c** 1#NT-350 °C. **d** 3#NT-350 °C

W^{6+} in WO_3 to W^{4+} (Zaki et al. 2011), and the reduction peak at about 800° is due to the reduction of W^{4+} to W^0. Compared to TiO_2-based catalysts, SiO_2-doped catalysts gave a reduction peak about 25 °C closer to the low-temperature zone (Pan et al. 2013) because of the good dispersity of vanadium and the interaction between vanadium and the TiO_2 support (Zhao et al. 2010). Furthermore, the peak area of the SiO_2-doped catalysts is larger, demonstrating superior reducibility of the catalyst and higher potential for redox reactions (Youn et al. 2015).

3.2.6 NH_3-TPD Analysis

In SCR deNO_x reactions, NH_3 is first adsorbed on the surface-active sites of the catalyst and then reacts with NO in the adsorbed state or gaseous state. Therefore, the adsorption capacity of the catalyst for NH_3 is the critical factor that influences the NO_x conversion efficiency. Figure 9 shows the TPD results for the 3V-10W/1#NT-650 °C and 3V-10W/3#NT-650 °C catalysts. There are three distinct desorption peaks for the 3V-10W/1#NT-650 °C catalyst and two distinct desorption peaks for the 3V-10W/3#NT-650 °C catalyst. The peak around 110 °C with higher amplitude and long duration corresponds to the Brønsted acid sites. The other peak around 470 °C with lower amplitude corresponds to the Lewis acid sites (Srnak et al. 1992). According to the test results, we can see a great increase in Brønsted acidity and a slight decrease in Lewis acidity after Si addition. Peaks observed around 720 °C are attributed to N_2 desorption (Wang 2006). The surface acidity of the catalyst is enhanced by the introduction of SiO_2 (Japke et al. 2015). The new acidic sites are assumed to be produced by charge imbalance localized at the Si–O–Ti bonds owing to the difference in coordination geometries of Si and Ti (Millini et al. 1992).

4 Conclusion

In this work, a series of mV-10W/n#NT-T nanotube catalysts were prepared, where m indicates the V_2O_5 loading, n#NT is an identifier of the TiO_2-SiO_2

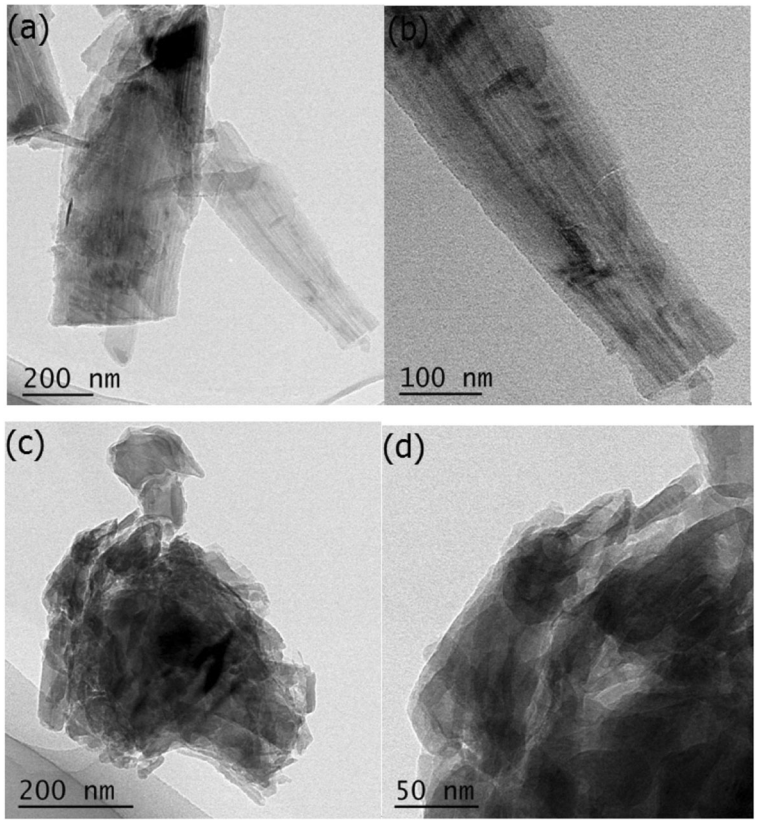

Fig. 7 Catalyst TEM diagrams. **a**, **b** 3V-10W/3#NT-450 °C. **c**, **d** 3V-10W/3#NT-650 °C

nanotube support with a specific SiO_2/TiO_2 molar ratio, and T is the catalyst calcination temperature. Experimental results indicated that SiO_2-doped nanotube catalysts have higher NO conversion efficiencies and wider reaction windows. Among all these catalysts, the 3V-10W/3#NT-650 °C nanotube catalyst demonstrated the highest NO conversion efficiency. At a gas hourly space velocity (GHSV) of 100,000 h^{-1} and over the reaction temperature range 300–500 °C, the NO conversion efficiency could reach 100%. The efficiency is higher than that of TiO_2 nanotube catalysts by over 30% at 350 °C. The NO conversion efficiency could still exceed 94.5% with the introduction of SO_2 and H_2O into the reaction system at a GHSV of 200,000 h^{-1} and a temperature of

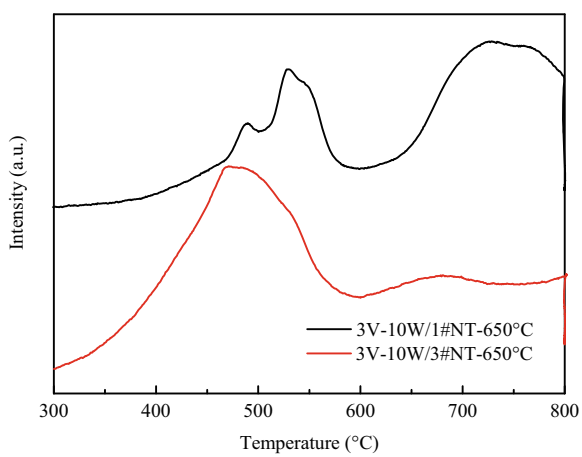

Fig. 8 H_2-TPR spectrum of catalyst

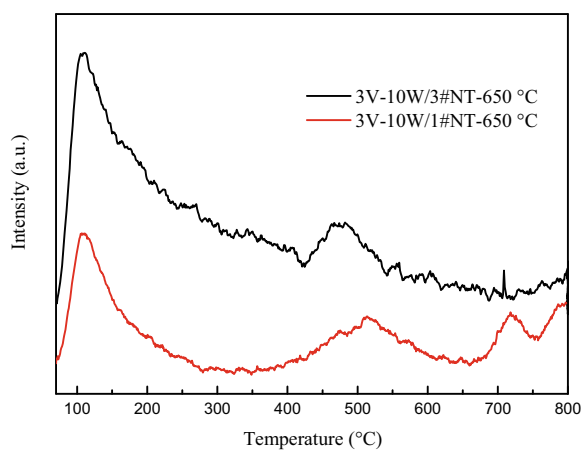

Fig. 9 NH_3-TPD spectrum of catalyst

300 °C. The BET and XRD results reveal that formation of the nanotube structure increased the catalyst BET surface area by more than 250%. The TiO_2 in the SiO_2-doped support is completely in the anatase phase, and no V_2O_5 characteristic diffraction peaks were detected, showing that V_2O_5 possessed good dispersity on the TiO_2-SiO_2 support, which was also confirmed by TEM. As indicated by NH_3-TPD and H_2-TPR measurements, the total acidity and redox capacity of the nanotube catalysts were enhanced after doping with Si.

Acknowledgments This work was supported by the K.C. Wong Magna Fund in Ningbo University and the National 863 High Technology Research Program of China [Grant No. 2008AA05Z205].

References

Camposeco, R., Castillo, S., Mugica, V., Centeno, I., & Marin, J. (2014). Role of V_2O_5-WO_3/$H_2Ti_3O_7$-nanotube-model catalysts in the enhancement of the catalytic activity for the SCR-NH3 process. *Chemical Engineering Journal, 242*(8), 313–320.

Chen, X. B., Cao, S., Weng, X. L., Wang, H. Q., & Wu, Z. B. (2012). Effects of morphology and structure of titanate supports on the performance of ceria in selective catalytic reduction of NO. *Catalysis Communications, 26*(35), 178–182.

Cheng, K., Liu, J., Zhang, T., Li, J. M., Zhao, Z., Wei, Y. C., et al. (2014). Effect of Ce doping of TiO_2 support on NH_3-SCR activity over V_2O_5-WO_3/CeO_2-TiO_2 catalyst. *Journal of Environmental Sciences, 26*(10), 2106–2113.

Choung, J. W., Nam, I. S., & Ham, S. W. (2006). Effect of promoters including tungsten and barium on the thermal stability of V_2O_5/sulfated TiO_2 catalyst for NO reduction by NH_3. *Catalysis Today, 111*(3–4), 242–247.

Dong, R. L., Na, C., Zhang, H. P., Chen, Z. D., & Jin, C. C. (2016). TiO_2/SiO_2 mesoporous microspheres with intelligently controlled texture. *Materials and Design, 89*, 830–838.

Fan, Y. Z., & Cao, F. H. (2011). Thermal decomposition kinetics of ammonium sulfate. *Journal of Chemical Engineering of Chinese Universities, 25*(2), 34l–346 (in Chinese).

Fang, N., Li, X. Y., & Jia, J. P. (2007). TiO_2 nano-tube modified by SiO_2: its preparation and photocatalytic abilities. *Environmental Science & Technology, 30*(3), 34-35+40+1 (in Chinese).

Forzatti, P. (2001). Present status and perspectives in de-NOx SCR catalysis. *Applied Catalysis A: General, 222*(1–2), 221–236.

Gao, X. T., Bare, S. R., Fierro, J. L. G., & Wachs, I. E. (1999). Structural characteristics and reactivity/reducibility properties of dispersed and bilayered V_2O_5/TiO_2/SiO_2 catalysts. *The Journal of Physical Chemistry, 103*(4), 618–629.

Huang, Z. G., Liu, Z. Y., Zhang, X. L., & Liu, Q. Y. (2006). Inhibition effect of H_2O on V_2O_5/AC catalyst for catalytic reduction of NO with NH_3 at low temperature. *Applied Catalysis B: Environmental, 63*(3–4), 260–265.

Japke, E., Casapu, M., Trouillet, V., Deutschmann, O., & Grunwaldt, J. D. (2015). Soot and hydrocarbon oxidation over vanadia-based SCR catalysts. *Catalysis Today, 258*, 461–469.

Jin, R. B., Wu, Z. B., Liu, Y., Jiang, B., & Wang, H. (2009). Photocatalytic reduction of NO with NH3 using Si-doped TiO_2 prepared by hydrothermal method. *Journal of Hazardous Materials, 161*(1), 42–48.

Kobayashi, M., Kuma, R., Masaki, S., & Sugishima, N. (2005). TiO_2-SiO_2 and V_2O_5/TiO_2-SiO_2 catalyst: physico-chemical characteristics and catalytic behavior in selective catalytic reduction of NO by NH_3. *Applied Catalysis B: Environmental, 60*(3–4), 173–179.

Kristensen, S. B., Kunov-Kruse, A. J., Riisager, A., Rasmussen, S. B., & Fehrmann, R. (2011). High performance vanadia–anatase nanoparticle catalysts for the selective catalytic reduction of NO by ammonia. *Journal of Catalysis, 284*, 60–67.

Liu, X. S., Wu, X. D., Xu, T. F., Weng, D., Si, Z. C., & Ran, R. (2016). Effects of silica additive on the NH_3-SCR activity and thermal stability of a V_2O_5/WO_3-TiO_2 catalyst. *Chinese Journal of Catalysis, 37*(8), 1340–1346.

Madia, G., Elsener, M., Koebel, M., Raimondi, F., & Wokaun, A. (2002). Thermal stability of vanadia-tungsta-titania catalysts in the SCR process. *Applied Catalysis B: Environmental, 39*(2), 181–190.

Millini, R., Massara, E. P., Perego, G., & Bellussi, G. (1992). Framework composition of titanium silicalite-1. *Journal of Catalysis, 137*(2), 497–503.

Morin, S., Savarino, J., Frey, M. M., Yan, N., & Bekki, S. (2008). Tracing the origin and fate of NOx in the Arctic atmosphere using stable isotopes in nitrate. *Science, 322*(5902), 730–732.

Nova, I., Acqua, L., Lietti, L., Giamello, E., & Forzatti, P. (2001). Study of thermal deactivation of a de-NO_X commercial catalyst. *Applied Catalysis B: Environmental, 35*(1), 31–42.

Odenbrand, C. U. I. (2008). Thermal stability of vanadia SCR catalysts for the use in diesel applications. *Chemical Engineering Research and Design, 86*(7), 663–672.

Pan, Y. X., Zhao, W., Zhong, Q., Cai, W., & Li, H. Y. (2013). Promotional effect of Si-doped V_2O_5/TiO_2 for selective catalytic reduction of NOx by NH3. *Journal of Environmental Sciences, 25*(8), 1703–1711.

Pang, L., Fan, C., Shao, L. N., Yi, J. X., Cai, X., Wang, J., et al. (2014). Effect of V_2O_5/WO_3-TiO_2 catalyst preparation method on NOx removal from diesel exhaust. *Chinese Journal of Catalysis, 35*(12), 2020–2028.

Putluru, S. S. R., Schill, L., Godiksen, A., Poreddy, R., Mossin, S., Jensen, A. D., & Fehrmann, R. (2016). Promoted V_2O_5/TiO_2 catalysts for selective catalytic reduction of NO with NH_3 at low temperatures. *Applied Catalysis B: Environmental, 183*, 282–290.

Shen, B. X., & Ma, J. (2012). Alkali-resistant performance of V_2O_5-WO_3/TiO_2 catalyst modified by SiO_2. *Journal of Fuel Chemistry and Technology, 40*(2), 247–251 (in Chinese).

Shi, A. J., Wang, X. Q., Yu, T., & Shen, M. Q. (2011). The effect of zirconia additive on the activity and structure stability of V_2O_5/WO_3-TiO_2 ammonia SCR catalysts. *Applied Catalysis B: Environmental, 106*(3–4), 359–369.

Srnak, T. Z., Dumesic, J. A., Clausen, B. S., Törnqvist, E., & Topsøet, N. Y. (1992). Temperature-programmed desorption/

reaction and in situ spectroscopic studies of vanadia/titania for catalytic reduction of nitric oxide. *Journal of Catalysis, 135*(30), 246–262.

Su, Y., Chen, S., Quan, X., Zhao, H. M., & Zhang, Y. B. (2008). A silicon-doped TiO_2 nanotube arrays electrode with enhanced photoelectron catalytic activity. *Applied Surface Science, 255*(5), 2167–2172.

Tang, N., Chen, X. B., Mo, J. S., Wang, H. Q., & Wu, Z. B. (2013). Influence of calcination temperature on the selective catalytic reduction performance and physicochemical properties of ceria doped titanate nanotubes. *Proceedings of the CSEE, 33*(29), 33–37 (in Chinese).

Tao, J. Z., Li, G. X., & Tong, D. H. (2008). Effects of H_2O and SO_2 on NOx selective catalytic reduction by NH3. *Chinese Internal Combustion Engine Engineering, 29*(3), 56–58.

Tran, T., Yu, J., Gan, L., Guo, F., Phan, D., & Xu, G. W. (2016). Upgrading V_2O_5-WO_3/TiO_2 deNOx catalyst with TiO_2-SiO_2 support prepared from Ti-bearing blast furnace slag. *Catalysts, 6*(4), 1–14.

Vedrine, J. C. (2000). Industrial features. *Catalysis Today, 56*(4), 333–334.

Wang, Y. (2006). Adsorption action of NO gas on the TiO_2 surface. *Acta Chimica Sinica, 64*(15), 1611–1614.

Wang, Y. F., & Sun, Y. P. (2011). Preparation, photocatalytic activity and mechanism of Si-doped titania material. *Journal of the Chinese Ceramic Society, 39*(2), 204–209.

Wang, H. Q., Chen, X. B., Weng, X. L., Liu, Y., Gao, S., & Wu, Z. B. (2011). Enhanced catalytic activity for selective catalytic reduction of NO over titanium nanotube-confined CeO_2 catalyst. *Catalysis Communications, 12*(11), 1042–1045.

Wang, C. Z., Yang, S. J., Chang, H. Z., Peng, Y., & Li, J. H. (2013). Dispersion of tungsten oxide on SCR performance of V_2O_5-WO_3/TiO_2: acidity, surface species and catalytic activity. *Chemical Engineering Journal, 225*, 520–527.

Weber, C. L., Jaramillo, P., Marriott, J., & Samaras, C. (2010). Life cycle assessment and grid electricity: what do we know and what can we know? *Environmental Science & Technology, 44*(6), 1895–1901.

Yao, Y., Zhang, S. L., Zhong, Q., & Liu, X. X. (2011). Low temperature selective catalytic reduction of NO over manganese supported on TiO_2 nanotubes. *Journal of Fuel Chemistry and Technology, 39*(9), 694–701 (in Chinese).

Youn, S., Song, I., & Kim, D. H. (2015). Promotional effect on selective catalytic reduction of NOx with NH_3 over overloaded W and Ce on V_2O_5/TiO_2 catalysts. *Journal of Nanomaterials, 2015*, 1–7.

Zaki, M. I., Fouad, N. E., Mansour, S. A. A., & Muftah, A. I. (2011). Temperature-programmed and X-ray diffractometry studies of hydrogen-reduction course and products of WO^3 powder: influence of reduction parameters. *Thermochimica Acta, 523*(1–2), 90–96.

Zhang, P., Chen, T. H., Zou, X. H., Zhu, C. Z., Chen, D., & Liu, H. B. (2014). V_2O_5/hematite catalyst for low temperature selective catalytic reduction of NOx with NH_3. *Chinese Journal of Catalysis, 35*(1), 99–107.

Zhao, H. Y., Bennici, S., Shen, J. Y., & Auroux, A. (2010). Nature of surface sites of V_2O_5-TiO_2/SO_4^{2-} catalysts and reactivity in selective oxidation of methanol to dimethoxymethane. *Journal of Catalysis, 272*(1), 176–189.